

## Status update: $\pi^0 \rightarrow \gamma^* \gamma^*$ transition form factor on CLS ensembles

---

**Jonna Koponen,<sup>a,\*</sup> Antoine Gérardin,<sup>b</sup> Harvey B. Meyer,<sup>a,c</sup> Konstantin Ottnad<sup>a</sup> and Georg von Hippel<sup>a</sup>**

<sup>a</sup>*PRISMA<sup>+</sup> Cluster of Excellence & Institut für Kernphysik, Johannes-Gutenberg-Universität Mainz, D-55099 Mainz, Germany*

<sup>b</sup>*Aix-Marseille Université, Université de Toulon, CNRS, CPT, Marseille, France*

<sup>c</sup>*Helmholtz-Institut Mainz, Johannes-Gutenberg-Universität Mainz, D-55099 Mainz, Germany*

*E-mail:* [jkoponen@uni-mainz.de](mailto:jkoponen@uni-mainz.de)

In this report we present the status of the Mainz group's lattice QCD calculation of the pion transition form factor, which describes the interaction of an on-shell pion with two off-shell photons. This form factor is the main ingredient in the calculation of the pion-pole contribution to hadronic light-by-light scattering in the muon  $g - 2$ .

We use the  $N_f = 2 + 1$  CLS gauge ensembles, and we update our previous work by including a physical pion mass ensemble (E250). We compute the transition form factor in a moving frame as well as in the pion rest frame in order to have access to a wider range of photon virtualities. In addition to the quark-line connected correlator we also compute the quark-line disconnected diagrams that contribute to the form factor.

At the final stage of the analysis, the result on E250 will be combined with the previous work published in 2019 to extrapolate the form factor to the continuum and to physical quark masses.

*The 40th International Symposium on Lattice Field Theory (Lattice 2023)  
July 31st - August 4th, 2023  
Fermi National Accelerator Laboratory*

---

\*Speaker

## 1. Introduction and motivation

The transition form factor (TFF)  $\mathcal{F}_{\pi^0 \gamma^* \gamma^*}$  describes the interaction of an on-shell pion with two off-shell photons. It is the main ingredient in the calculation of the pion-pole contribution to hadronic light-by-light scattering in the muon  $g - 2$ . There is also a direct relation between  $\mathcal{F}_{\pi^0 \gamma^* \gamma^*}(0, 0)$  (the transition form factor with two real photons) and the partial decay width  $\Gamma(\pi^0 \rightarrow \gamma\gamma)$  (see Eq. (13) in Section 3). In the leading order of chiral perturbation theory ( $\chi$ PT),

$$\Gamma(\pi^0 \rightarrow \gamma\gamma) = \frac{m_{\pi^0}^3 \alpha_e^2 N_c^2}{576 \pi^3 F_{\pi^0}^2}, \quad (1)$$

where  $\alpha_e$  is the fine structure constant,  $N_c$  is the number of colors and  $F_{\pi^0}$  is pion decay constant in the chiral limit. There is a tension between the measured value and the theoretical predictions when NLO corrections are added, which is illustrated very clearly for example in Fig. 72 in [1]. Lattice calculations could shed light to this issue, if 2% precision can be achieved on the normalization of the TFF.

## 2. Extraction of the TFF

The calculation follows very closely the Mainz group's publication [2] (see also [3]). The transition form factor is extracted from matrix elements

$$M_{\mu\nu}(p, q_1) = i \int d^4x e^{iq_1 \cdot x} \langle 0 | T \{ J_\mu(x) J_\nu(0) \} | \pi^0(p) \rangle = \epsilon_{\mu\nu\alpha\beta} q_1^\alpha q_2^\beta \mathcal{F}_{\pi^0 \gamma^* \gamma^*}(q_1^2, q_2^2), \quad (2)$$

where  $J_\mu$  is the electromagnetic (EM) current. Here  $q_1 = (\omega_1, \vec{q}_1)$  and  $q_2 = (E_\pi - \omega_1, \vec{p} - \vec{q}_1)$  are the four-momenta associated with the two currents, and  $p$  is the four-momentum of the pion, such that  $p = q_1 + q_2$ .

To cover a wide range of photon virtualities, we use both the rest frame of the pion,  $\vec{p} = (0, 0, 0)$ , and a moving frame  $\vec{p} = (0, 0, 1)$  (in units of  $2\pi/L$ ). The increase in the range of accessible virtualities is best illustrated in the  $(q_1^2, q_2^2)$ -plane — see Fig. 1. Each curve in the plot represents a fixed value of  $\vec{q}_1$  and  $\vec{p}$ , and  $\omega_1$  is a free parameter (this tracks the curve from one end to another).

The Euclidean matrix elements read

$$M_{\mu\nu} = (i^{n_0}) M_{\mu\nu}^E, \quad M_{\mu\nu}^E = - \int_{-\infty}^{\infty} d\tau e^{\omega_1 \tau} \int d^3z e^{-i\vec{q}_1 \cdot \vec{x}} \langle 0 | T \{ J_\mu(\vec{x}, \tau) J_\nu(\vec{0}, 0) \} | \pi^0(p) \rangle, \quad (3)$$

where  $n_0$  denotes the number of temporal indices. The matrix elements can be obtained by integration over an Euclidean time dependent amplitude,

$$M_{\mu\nu}^E(p, q_1) = \frac{2E_\pi}{Z_\pi} \int_{-\infty}^{\infty} d\tau e^{\omega_1 \tau} \tilde{A}_{\mu\nu}(\tau), \quad (4)$$

where  $\tau = t_i - t_f$  is the time separation between the two EM currents. The amplitude  $\tilde{A}_{\mu\nu}(\tau)$  is connected to a 3-point correlator calculated on the lattice by

$$C_{\mu\nu}^{(3)}(\tau, t_\pi) \equiv a^6 \sum_{\vec{x}, \vec{z}} \langle J_\mu(\vec{x}, t_i) J_\nu(\vec{0}, t_f) P^\dagger(\vec{z}, t_0) \rangle e^{i\vec{p} \cdot \vec{z}} e^{-i\vec{q}_1 \cdot \vec{x}} \quad (5)$$

$$\tilde{A}_{\mu\nu}(\tau) \equiv \lim_{t_\pi \rightarrow +\infty} e^{E_\pi(t_f - t_0)} C_{\mu\nu}^{(3)}(\tau, t_\pi), \quad (t_0 < t_f), \quad (6)$$

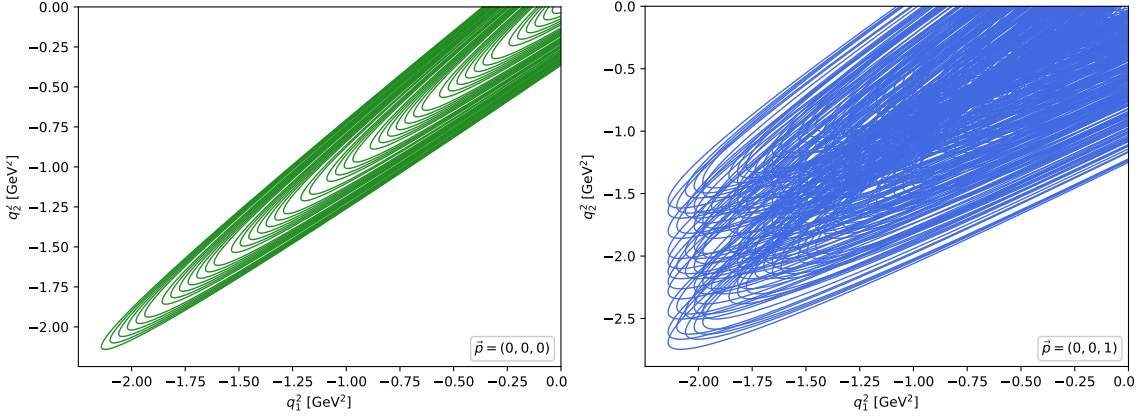


**Figure 1:** Photon virtualities at the physical pion mass with  $L \approx 6$  fm.

where  $t_\pi$  is the time separation between the pion and the closest EM current. In addition to the quark-line connected diagram, there are contributions from two quark-line disconnected diagrams that have to be calculated. Both the connected and disconnected diagrams are depicted in Fig. 2.

## 2.1 Lattice ensembles

We use the CLS  $N_f = 2+1$  ensembles with non-perturbatively  $\mathcal{O}(a)$ -improved Wilson fermions and tree-level improved Lüscher-Weisz gauge action. We have four lattice spacings and use multiple pion masses to control the chiral extrapolation. All ensembles have fairly large volumes ( $M_\pi L \geq 4$ ). More details about the ensembles can be found in [2] and references therein. Compared to the publication [2] we now add one ensemble (E250) at the physical pion mass with a lattice spacing of  $a \approx 0.064$  fm, size  $96^3 \times 192$  and  $L \approx 6$  fm.

## 2.2 Correlators

Recall that  $\tilde{A}_{\mu\nu}(\tau)$  is directly related to the 3-point correlators  $C_{\mu\nu}^{(3)}$ . For convenience we define two scalar functions  $\tilde{A}^{(1)}(\tau)$  and  $\tilde{A}^{(2)}(\tau)$ :

$$\begin{aligned} \tilde{A}_{0k}(\tau) &= (\vec{q}_1 \times \vec{p})_k \tilde{A}^{(1)}(\tau), \\ \epsilon'^k \tilde{A}_{kl}(\tau) \epsilon^l &= -i(\vec{\epsilon}' \times \vec{\epsilon}) \cdot \left( \vec{q}_1 E_\pi \tilde{A}^{(1)}(\tau) + \vec{p} \frac{d\tilde{A}^{(1)}(\tau)}{d\tau} \right). \end{aligned} \quad (7)$$

In the moving frame we define for simplicity  $\tilde{A}_{12}(\tau) \equiv -iE_\pi p_z \tilde{A}^{(2)}(\tau)$ . The two scalar functions have very distinct features as can be seen in Fig. 3:  $\tilde{A}^{(1)}$  peaks at  $\tau = 0$ , whereas  $\tilde{A}^{(2)}$  changes

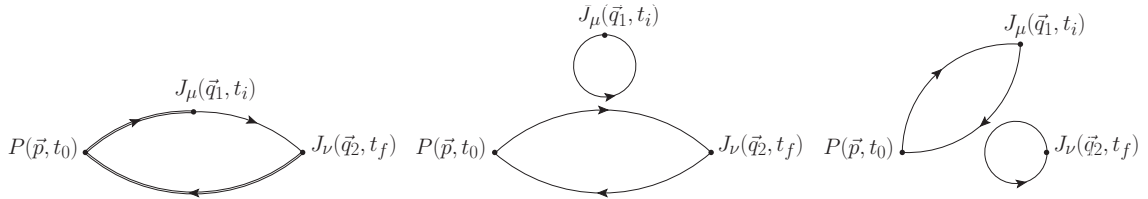


**Figure 2:** Connected and disconnected diagrams.

sign. See section 2.4 for more details of the two fits, VMD and LMD, that are used to model the tail contribution.

### 2.3 Disconnected contribution

In addition to the quark-line connected piece, we need two quark-line disconnected diagrams. The quark loops are computed using stochastic all-to-all methods [4–6], while the two-point functions are computed using point sources. We find the disconnected contribution

$$\Delta F(-Q_1^2, -Q_2^2) = \frac{\mathcal{F}_{\pi^0 \gamma^* \gamma^*}^{\text{disc}}(-Q_1^2, -Q_2^2)}{\mathcal{F}_{\pi^0 \gamma^* \gamma^*}^{\text{conn}}(-Q_1^2, -Q_2^2)} \quad (8)$$

is at the few-percent level. This is illustrated in Fig. 4, where the plot on the left shows the connected piece and the disconnected piece (multiplied by ten) for the scalar function  $\tilde{A}^{(1)}$ , whereas the plot on the right shows the ratio given in Eq. (8).

### 2.4 Modeling the tail

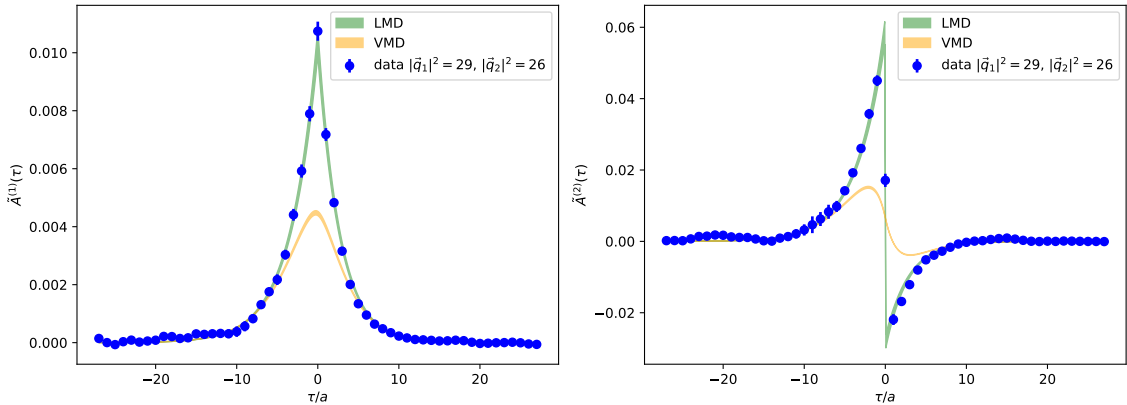
Recall that we extract the TFF by evaluating the integral  $\int_{-\infty}^{\infty} d\tau e^{\omega_1 \tau} \tilde{A}_{\mu\nu}(\tau)$ . We need to model  $\tilde{A}_{\mu\nu}(\tau)$  at large  $|\tau|$  to get the tail contribution. We use two models:

- Lowest Meson Dominance (LMD)

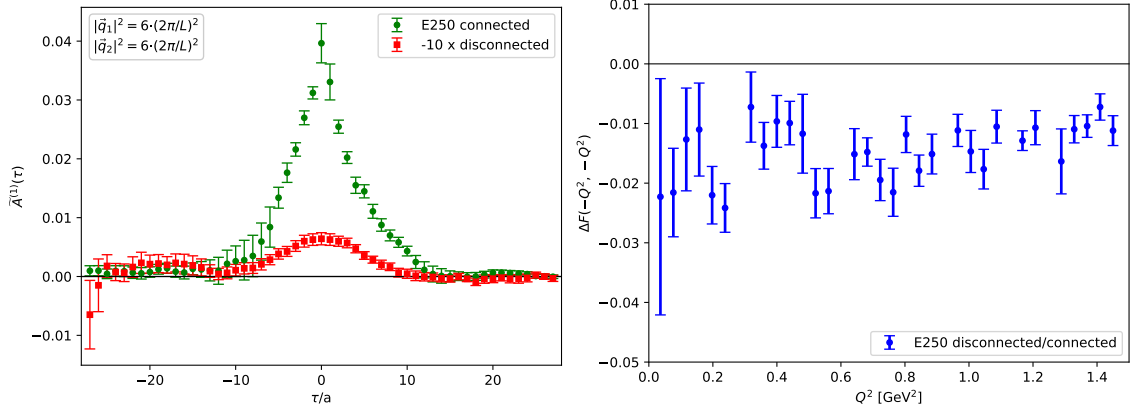
$$\tilde{A}_{\mu\nu}^{\text{LMD}}(\tau) = \frac{Z_\pi}{4\pi E_\pi} \int_{-\infty}^{\infty} d\tilde{\omega} \frac{(P_{\mu\nu}^E \tilde{\omega} + Q_{\mu\nu}^E) (\alpha M_V^4 + \beta(q_1^2 + q_2^2))}{(\tilde{\omega} - \tilde{\omega}_1^{(+)}) (\tilde{\omega} - \tilde{\omega}_1^{(-)}) (\tilde{\omega} - \tilde{\omega}_2^{(+)}) (\tilde{\omega} - \tilde{\omega}_2^{(-)})} e^{-i\tilde{\omega}\tau} \quad (9)$$

with

$$\begin{aligned} P_{\mu\nu}^E &= i\epsilon_{\mu\nu 0i} P^i, & \tilde{\omega}_1^{(\pm)} &= \pm i \sqrt{M_V^2 + |\vec{q}_1|^2}, \\ Q_{\mu\nu}^E &= \epsilon_{\mu\nu i0} E_\pi q_1^i - i\epsilon_{\mu\nu ij} q_1^i p^j, & \tilde{\omega}_2^{(\pm)} &= -i \left( E_\pi \mp \sqrt{M_V^2 + |\vec{q}_2|^2} \right), \end{aligned}$$



**Figure 3:** Examples of the connected contribution to the scalar functions  $\tilde{A}^{(1)}(\tau)$  and  $\tilde{A}^{(2)}(\tau)$ . The momenta are given in units of  $2\pi/L$ .


**Figure 4:** Disconnected contribution.

and  $Z_\pi$  the overlap factor from the pion 2-point function. This gives an explicit expression for  $\widetilde{A}_{\mu\nu}^{\text{LMD}}$ , which we use to fit our data using  $\alpha$ ,  $\beta$  and  $M_V$  as fit parameters.

- Vector Meson Dominance (VMD): Set  $\beta = 0$  in the LMD model

These models are used at  $|\tau|/a > 20$  ( $|\tau| > 1.3$  fm), to make sure the contribution from the tail is small compared to the contribution we extract directly from our lattice data. Both VMD and LMD model fits to the data are shown in Fig. 3. Especially the latter model describes the data well even fairly close to  $\tau = 0$ , and we include data  $|\tau|/a \geq 8$  ( $|\tau| \geq 0.5$  fm) in these fits.

## 2.5 Parameterizing the form factor: $z$ -expansion

After obtaining the transition form factor at several virtualities  $(q_1^2, q_2^2) \equiv (-Q_1^2, -Q_2^2)$ , we parameterize it using a conformal mapping

$$z_k = \frac{\sqrt{t_{\text{cut}} + Q_k^2} - \sqrt{t_{\text{cut}} - t_0}}{\sqrt{t_{\text{cut}} + Q_k^2} + \sqrt{t_{\text{cut}} - t_0}}, \quad \text{with } t_{\text{cut}} = 4(m_\pi^{\text{phys}})^2, \quad \text{and } t_0 = t_{\text{cut}} \left( 1 - \sqrt{1 + \frac{Q_{\text{max}}^2}{t_{\text{cut}}}} \right). \quad (10)$$

The form factor is then written as an expansion in  $z_1$  and  $z_2$ :

$$P(Q_1^2, Q_2^2) \mathcal{F}_{\pi^0 \gamma^* \gamma^*}(-Q_1^2, -Q_2^2) = \sum_{n,m=0}^N c_{nm} \left( z_1^n + (-1)^{N+n} \frac{n}{N+1} z_1^{N+1} \right) \left( z_2^m + (-1)^{N+m} \frac{m}{N+1} z_2^{N+1} \right), \quad (11)$$

where the coefficients  $c_{nm} = c_{mn}$ , the fit parameters, are symmetric. The polynomial

$$P(Q_1^2, Q_2^2) = 1 + \frac{Q_1^2 + Q_2^2}{M_V^2} \quad (12)$$

implements the vector meson pole with  $M_V = 775$  MeV and ensures the correct asymptotic behaviour at large virtualities.

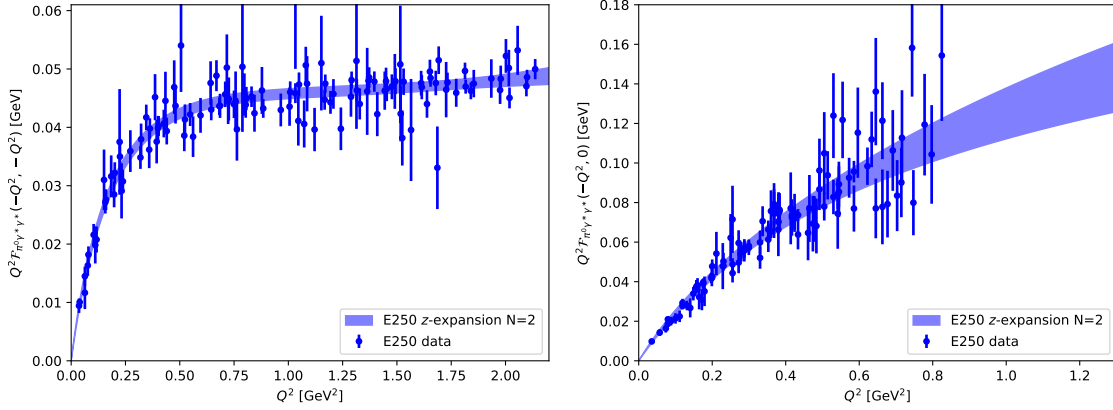


**Figure 5:** Transition form factor  $Q^2 \mathcal{F}_{\pi^0 \gamma^* \gamma^*}$ . On the left: double virtual  $Q^2 \mathcal{F}_{\pi^0 \gamma^* \gamma^*}(-Q^2, -Q^2)$ ; on the right: single virtual  $Q^2 \mathcal{F}_{\pi^0 \gamma^* \gamma^*}(-Q^2, 0)$ .

### 3. Results

Preliminary results for the transition form factor on the physical pion mass ensemble are plotted in Fig. 5 along with the  $N = 2$   $z$ -expansion. We plot our fit for two specific choices of  $\omega_1$ , that correspond to the double virtual  $Q_1^2 = Q_2^2 = Q^2$  and single virtual  $Q_1^2 = Q^2, Q_2^2 = 0$ , cases. The  $z$ -expansion with  $N = 2$  clearly describes the data well.

Let us then recall the relation between the partial decay width  $\Gamma(\pi^0 \rightarrow \gamma\gamma)$  and the transition form factor:

$$\Gamma(\pi^0 \rightarrow \gamma\gamma) = \frac{\pi \alpha_e^2 (m_{\pi^0})^3}{4} \mathcal{F}_{\pi^0 \gamma^* \gamma^*}^2(0, 0). \quad (13)$$

This can be used to convert the normalization of the pion transition form factor into an estimate of the decay width  $\Gamma(\pi^0 \rightarrow \gamma\gamma)$ , and the results are depicted in Fig. 6. The fit curves and data points plotted here are the same as in Fig. 5 (but without the factor of  $Q^2$ ), and we simply zoom in on the small- $Q^2$  region. Comparison to the experimental result by PrimEx and comparison with other lattice QCD results by BMW [7] and ETMC [8] shows we agree very well. Unfortunately, the lattice QCD results do not match the precision of the experimental result yet.

### 4. Summary and outlook

In this report, we have given a status update of the Mainz group's calculation of the pion transition form factor. The main development is the inclusion of a physical pion mass ensemble E250 with large volume. We compute the disconnected diagrams needed in addition to the quark-line connected piece to construct the full form factor. The new results presented here are still preliminary, and we plan to increase statistics. At the final stage of the analysis, the result on E250 will be combined with the previous work published in 2019 [2] to extrapolate the form factor to the continuum and to physical quark masses.

The transition form factor  $\mathcal{F}_{\pi^0 \gamma^* \gamma^*}$  is the main ingredient in the estimation of the pion-pole contribution to hadronic light-by-light scattering in the muon  $g - 2$ . The goal of this work is to improve this estimate by including E250 in the analysis. However, if lattice QCD calculations want

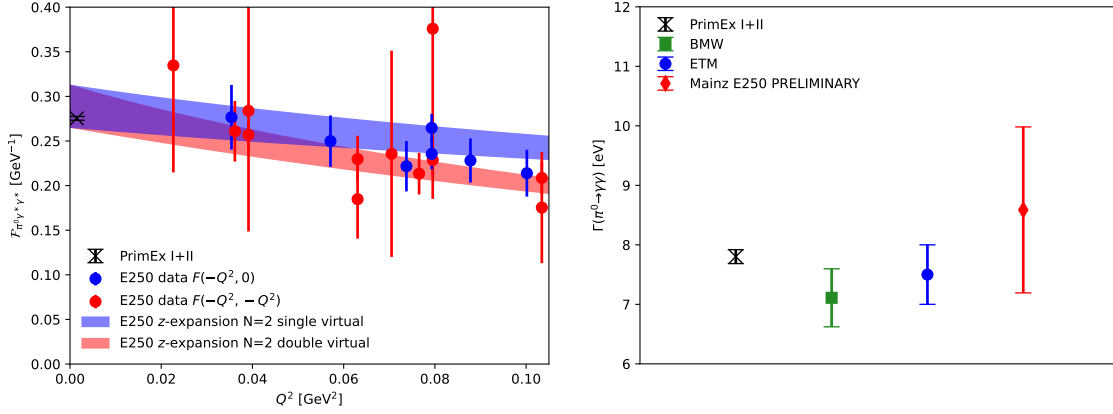


**Figure 6:** Connecting the behaviour of the TFF at  $Q^2 = 0$  with the partial decay width  $\Gamma(\pi^0 \rightarrow \gamma\gamma)$ . The experimental result by PrimEx was published in [9]. We also compare to other lattice QCD results from the BMW collaboration [7] and from the ETM collaboration [8].

to address the tension between the partial decay width  $\Gamma(\pi^0 \rightarrow \gamma\gamma)$  from the PrimEx-II experiment and NLO theory predictions, there is still a long way to go.

## Acknowledgments

The authors acknowledge the support of Deutsche Forschungsgemeinschaft (DFG) through project HI 2048/1-3 ‘‘Precise treatment of quark-sea contributions in lattice QCD’’ (project 399400745), through the research unit FOR 5327 ‘‘Photon-photon interactions in the Standard Model and beyond – exploiting the discovery potential from MESA to the LHC’’ (grant 458854507), and through the Cluster of Excellence ‘‘Precision Physics, Fundamental Interactions and Structure of Matter’’ (PRISMA+ EXC 2118/1) funded within the German Excellence Strategy (project ID 39083149). We thank our colleagues in the CLS initiative for sharing ensembles.

We acknowledge PRACE for awarding us access to HAWK at GCS@HLRS, Germany via application 2020225457. Parts of this research were conducted using the supercomputer MOGON 2 offered by Johannes Gutenberg University Mainz (hpc.uni-mainz.de), which is a member of the AHRP (Alliance for High Performance Computing in Rhineland Palatinate, www.ahrp.info) and the Gauss Alliance e.V. The authors gratefully acknowledge the Gauss Centre for Supercomputing e.V. (www.gauss-centre.eu) for funding this project by providing computing time on the GCS Supercomputer SuperMUC-NG at Leibniz Supercomputing Centre (www.lrz.de) and on the GCS Supercomputer JUWELS at Jülich Supercomputing Centre (JSC).

## References

- [1] A. Accardi, P. Achenbach, D. Adhikari, A. Afanasev, C. S. Akondi, N. Akopov, M. Albaladejo, H. Albataineh, M. Albrecht and B. Almeida-Zamora, *et al.* [arXiv:2306.09360 [nucl-ex]].
- [2] A. Gérardin, H. B. Meyer and A. Nyffeler, Phys. Rev. D **100** (2019) no.3, 034520 doi:10.1103/PhysRevD.100.034520 [arXiv:1903.09471 [hep-lat]].

- [3] A. Gérardin, H. B. Meyer and A. Nyffeler, Phys. Rev. D **94** (2016) no.7, 074507 doi:10.1103/PhysRevD.94.074507 [arXiv:1607.08174 [hep-lat]].
- [4] L. Giusti, T. Harris, A. Nada and S. Schaefer, Eur. Phys. J. C **79** (2019) no.7, 586 doi:10.1140/epjc/s10052-019-7049-0 [arXiv:1903.10447 [hep-lat]].
- [5] K. Jansen *et al.* [ETM], Eur. Phys. J. C **58** (2008), 261-269 doi:10.1140/epjc/s10052-008-0764-6 [arXiv:0804.3871 [hep-lat]].
- [6] A. Stathopoulos, J. Laeuchli and K. Orginos, SIAM J. Sci. Comput. **35** (2013) no.5, S299-S322 doi:10.1137/120881452 [arXiv:1302.4018 [hep-lat]].
- [7] A. Gérardin, W. E. A. Verplanke, G. Wang, Z. Fodor, J. N. Guenther, L. Lellouch, K. K. Szabo and L. Varnhorst, [arXiv:2305.04570 [hep-lat]].
- [8] C. Alexandrou, S. Bacchio, G. Bergner, S. Burri, J. Finkenrath, A. Gasbarro, K. Hadjiyianakou, K. Jansen, G. Kanwar and B. Kostrzewa, *et al.* [arXiv:2308.12458 [hep-lat]].
- [9] I. Larin *et al.* [PrimEx-II], Science **368** (2020) no.6490, 506-509 doi:10.1126/science.aay6641